

# Two extreme cases of polarization direction alignment, one of starlight and the other of radio QSOs

*Richard Shurtleff* \*

June 2, 2021

## Abstract

Starlight and radio waves from QSOs share the ability to be polarized. For many regions of the Milky Way the alignment of the polarization directions of starlight is evident. However, it is useful to have a numerical alignment function that can be used to judge the significance of the correlations. The Hub Test provides such a function. Surveying the Galaxy with data from two catalogs of polarized starlight, Heiles 2000 and Berdyugin 2014, reveals an unusually well-aligned region which is then studied in more detail. Applied to a catalog of polarized radio QSOs, Pelgrims 2014 which is in part derived from Jackson 2007, a survey reveals the most significantly aligned region, which is studied further. Stars and QSOs have contrasting characteristics in terms of distance, degree of polarization, and strength of the alignment. The two most significantly aligned samples of starlight and radio QSOs are analyzed here. The alignment of the starlight sample outperforms all other portions of the Galaxy at the scale of the survey, about ten degrees, while the QSO sample has its polarization directions focusing down on a point extremely close to the QSOs themselves on the sky.

Keywords: Polarization ; Alignment ; Large scale structure

## 1 Introduction

Partially polarized starlight traces Galactic Magnetic fields, helping to understand Galactic structure [1, 2] and to inform the physics of the contaminating dust [3, 4] that obscures more distant objects of interest, such as quasi stellar objects (QSOs). The linear polarization of electromagnetic emissions of QSOs [5, 6] provides, for example, evidence of correlations between polarization directions and large scale structure. [7, 8] Detailed maps of the polarized cosmic microwave background radiation provide another subject for alignment studies. [9] For a variety of reasons, the alignment of a set of polarized sources can be an interesting property.

In this article, we conduct surveys of polarized starlight and radio QSOs, selecting the most significantly aligned regions for study. The scale, about  $10^\circ$  on the sky, is much larger than scales of interest in the GIPS polarized starlight collection project [10] which made detailed observations in the region  $18^\circ \leq l \leq 56^\circ$  and  $-1^\circ \leq b \leq +1^\circ$ . However, one expects that similar analyses can be conducted at the finer scales.

Fortuitously, the starlight sample and the QSO sample display near extreme characteristics of alignment. The polarization directions of the starlight sample converge on a point that is far from the sources, while the polarization vectors of QSOs focus on a point that is quite near the sample. For the polarization position

---

\*affiliation and mailing address: Department of Sciences, Wentworth Institute of Technology, 550 Huntington Avenue, Boston, MA, USA, 02115, orcid.org/0000-0001-5920-759X, e-mail: shurtleff@wit.edu, momentummatrix@yahoo.com

angle data, this translates into position angles for the polarization vectors of the starlight that are tightly constrained. Conversely, the QSO position angles are spread out over a wide range that is consistent with parallax; different locations in the sample see the focus point from different angles.

Also, the strength of the alignment and the degree of polarization do not coincide. The QSOs' polarization vectors are weakly aligned compared to the polarization directions of the stars. Yet the degree of the polarization, the percent polarization, is much higher for the QSOs than the starlight. The two samples are discussed in Sec. 2.

The alignment of the starlight sample and that of the QSOs is judged by the Hub Test. Since the test may be unfamiliar, a summary is provided in Sec. 3 with related material in the Appendix. The idea is to extend the polarization directions out from the sources forming great circles that form patterns of convergence and divergence. The 'hubs' are the points of best convergence and maximum divergence.

Other tests, for example, the 'S' and 'Z' tests, Ref. [5,6,11], collect the sources' polarization directions together, rating how well these position angles agree. Such tests are not designed to find well-correlated polarization directions that focus down on a point that is close to the sources. Only samples with nearly parallel position angles and with necessarily distant convergence can be detected. The Hub Test can detect correlations of samples, like the QSO sample, in a way that complements other tests that detect other types of correlations.

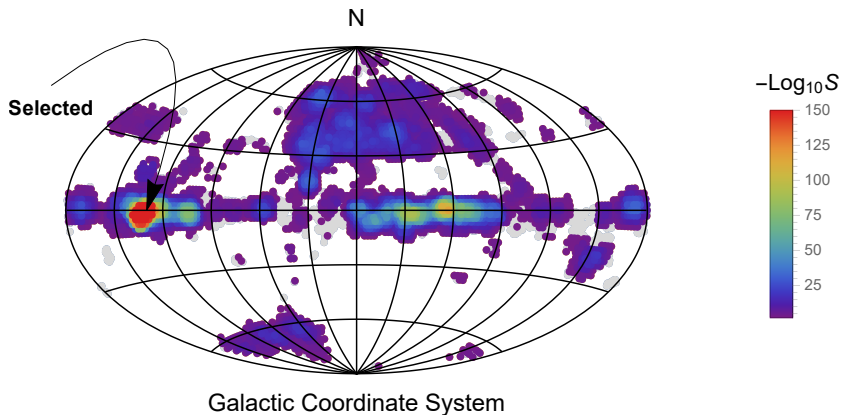


Figure 1: *Survey of polarized Galactic starlight.* The 5830 stars were grouped into  $5^\circ$  radius regions centered on grid points. The 3632 regions shown have at least 7 stars and are plotted as gray or color dots at the central grid point. Of these, 2983 regions are very significantly aligned, *i.e.*  $S \leq 0.01 = 10^{-2}$ , or, equivalently,  $-\log_{10} S \geq 2$  and those are plotted as color dots. The 22 selected regions have significance exponents above 150,  $-\log_{10} S \geq 150$ ; all regions above 150 are shaded red. Combining the 22 red-shaded regions gives the sample of 495 stars to be treated in detail. (Galactic coordinates centered on  $(l, b) = (0^\circ, 0^\circ)$ ;  $(+180^\circ, 0^\circ)$  on the left; an Aitoff plot; Color online.)

Two very significantly aligned samples are analyzed with the Hub test in Sec. 2. The first sample analyzes data found in two catalogs of polarized starlight, Heiles 2000 and Berdyugin 2014, [12,13]. The second sample analyzes data from Pelgrims 2014, which contains radio QSOs that are identified as QSOs in the large JVAS/CLASS 8.4Ghz catalog Jackson 2007. [11,14]

Sample	Coordinates	$N$	$\bar{\eta}_{\min}$	$H_{\min}$	Significance of $\bar{\eta}_{\min}$	$n\sigma$
Stars	Galactic	495	$6.966^\circ \pm 0.081^\circ$	$(41.8^\circ, 2^\circ) \pm (3.6^\circ, 1^\circ)$	$< 10^{-150} \approx 0$	48
QSOs	Equatorial	27	$21.76^\circ \pm 0.81^\circ$	$(9.7^\circ, 1.4^\circ) \pm (2.3^\circ, 2.5^\circ)$	$1.2_{-0.9}^{+3.0} \times 10^{-5}$	4.3

Table 1: *Alignment metrics.*

Concluding remarks are presented in Sec. 4. The most notable characteristic of the star sample alignment is its impressive quality, much better aligned than the second best-aligned and the other, lesser aligned, regions of the Galaxy. The QSOs' polarization direction alignment is thought to be innate, not due to the intervening dust. [7, 8] The QSO alignment is therefore, by definition, a large scale property.

## 2 Examples of extreme alignments

In this section, two samples are discussed. One has the polarization directions narrowly constrained and the alignment hubs are far from the sources. The second sample has polarizations directions pointing to a hub located near the sources and parallax forces the polarization directions to have a wide range of position angles.

The first sample consists of Milky Way stars. The polarized starlight data is taken from two catalogs, Heiles 2000 and Berdyugin 2014, [12, 13]. To get a general idea of the alignment of polarized starlight, we conduct a survey. A collection of  $5^\circ$ -radius regions are created centered on the grid points of a  $2^\circ \times 2^\circ$  mesh. The regions are populated with stars from the catalogs.

A kind of “topographical” map of the alignment of polarized Milky Way starlight is presented in Fig. 1. Fig. 1 is arranged so that higher elevations indicate more significant alignment. The trick is to make altitude a function of significance. Significance is difficult to plot, so the altitudes  $h$  in Fig. 1 are the negative log of significance, “the significance exponent”,

$$h(S) = -\log_{10} S. \quad (1)$$

The highest peak on the left tops off at  $h \approx 270$  and that means the significance  $S \approx 10^{-270}$ , essentially nil.

The sample consists of the best aligned regions in Fig. 1, those with significance exponent  $h \geq 150$ . All of these  $5^\circ$ -radius regions have  $S \leq 10^{-150} \approx 0$  and thus, in Fig. 1 their altitude  $h$  is at least 150,  $h \geq 150$ . Compared with the other regions, the alignment is amazing. One wonders what physical process can exert such dominating control on the polarization directions of the light from the stars on this patch of the sky.

The  $5^\circ$ -radius regions selected for study have centers  $(l, b)$  with  $115^\circ \leq l \leq 145^\circ$ ,  $-10^\circ \leq b \leq +10^\circ$ , and  $h = -\log_{10}(S) \geq 150$ . Together, the 22 selected  $5^\circ$ -radius regions contain 495 stars.

The alignment function  $\bar{\eta}(H)$  for the 495-star sample is depicted in Fig. 2 and calculated with Eq. (5). Note how the direction of best alignment, as indicated by the grey line through the blue shaded areas, follows the disk of the Galaxy. And the direction of most avoidance, indicated by the gray line toward the poles, is almost a great circle along constant longitude, a Galactic meridian.

The closest alignment hub  $H_{\min}$  sits in a convergence region on the sphere well away from the sources. The angular separation on the sky is  $88^\circ$  from the sample's center to  $H_{\min}$ , which is just  $2^\circ$  short of the largest possible value. By the symmetry across diameters, anything beyond  $90^\circ$  would make  $-H_{\min}$  closer

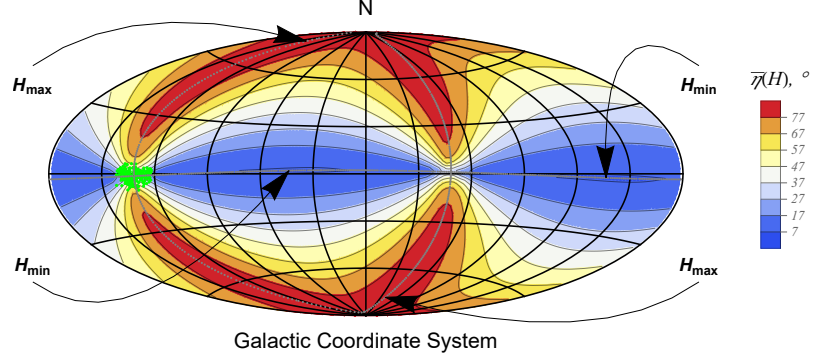


Figure 2: *The alignment function  $\bar{\eta}(H)$ , Eq. 5.* The sources are located at the green dots. To guide the eye, two Great Circles are drawn, one through the sources' center and the avoidance hubs  $\pm H_{\max}$ , while the other connects the sources' center with the alignment hubs  $\pm H_{\min}$ . The two Great Circles are shaded Gray, are perpendicular where they cross, and coincide with the structure of the Galaxy. (Galactic coordinates, an Aitoff plot, Color online.)

Sample	Coordinates	$N$	$\bar{\eta}_{\max}$	$H_{\max}$	Significance of $\bar{\eta}_{\max}$	$n\sigma$
Stars	Galactic	495	$83.13^\circ \pm 0.080^\circ$	$(140.5^\circ, 77.4^\circ) \pm (2.2^\circ, 2.7^\circ)$	$< 10^{-150} \approx 0$	48
QSOs	Equatorial	27	$66.03^\circ \pm 0.94^\circ$	$(144.^\circ, -25.^\circ) \pm (20.^\circ, 14.^\circ)$	$2.0_{-1.4}^{+3.6} \times 10^{-4}$	3.6

Table 2: *Avoidance metrics.*

to the sample's center than  $H_{\min}$ . Therefore the 495-star sample exemplifies an extreme case of alignment, the case with the alignment hub as far from the sources as possible.

Comparing the observed alignment angles  $\bar{\eta}_{\min}$  and  $\bar{\eta}_{\max}$  with the results with random polarization directions is necessary to determine the significance of the alignment. Since the statistical formulas in the Appendix depend on the size of the region and since the angular separation of the furthest star from the sample center is  $11.84^\circ$ , we choose the constants  $a_i$  and  $c_i$  in Table A1 for regions with radii  $\rho = 12^\circ$ .

As one should expect, 495 randomly directed vectors would average to the middle value,  $45^\circ$ , a little above  $45^\circ$  for avoidance and a little lower than  $45^\circ$  for alignment. By (A-3), one finds that, with randomly directed polarizations  $\psi^{\text{Random}}$ , the expected smallest alignment angle is  $\bar{\eta}_{\min}^{\text{Random}\psi} = 42.74^\circ \pm 0.75^\circ$  (Random  $\psi$ ). The expected largest avoidance angle is  $\bar{\eta}_{\max}^{\text{Random}\psi} = 47.27^\circ \pm 0.75^\circ$  (Random  $\psi$ ). The observed values  $\bar{\eta}_{\min} = 7^\circ$  and  $\bar{\eta}_{\max} = 83^\circ$  are far from random.

The correlation measure of alignment is the smallest alignment angle  $\bar{\eta}_{\min}$  and the measure of avoidance is the largest avoidance angle  $\bar{\eta}_{\max}$ . From Tables 1 and 2, we see that the smallest alignment angle  $\bar{\eta}_{\min}$  is about  $7^\circ$  and the largest avoidance angle  $\bar{\eta}_{\max}$  is  $83^\circ$ . Comparing both with the random run results, shows that both are about  $\Delta\eta/\sigma = 36^\circ/0.75^\circ = 48\sigma$ s from the random run means. One can reasonably conclude that the alignment and avoidance correlations of the sample's polarization directions are not due to chance.

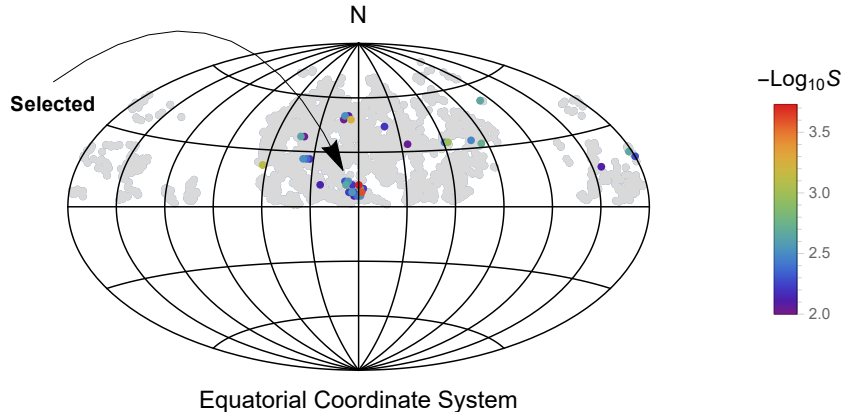


Figure 3: *Survey of polarized radio QSOs.* The 1450 QSOs were grouped into  $5^\circ$  radius regions centered on grid points. Those regions having at least 7 QSOs are plotted as gray dots at the central grid point. Just 35 regions showed very significant alignment, i.e.  $S \leq 0.01 = 10^{-2}$ , or, equivalently,  $-\log_{10} S \geq 2.0$ , and these are plotted as color dots. The indicated clump of 14 regions was selected for the analysis. There are 27 QSOs in the combined area of the 14 regions. (Equatorial coordinates centered on  $(\alpha, \delta) = (180^\circ, 0^\circ)$ , with  $(360^\circ, 0^\circ)$  on the right, an Aitoff plot, Color online.)

The star sample, with its hubs located so far away, is an example whose sources have nearly equal polarization directions, as shown in the position angle histogram in Fig. 5(a). That makes their alignment evident. Alignment tests that compare polarization directions directly, such as the S and Z tests, would agree that the polarization directions for this sample are very significantly aligned. One concludes that the Hub test and the S and Z tests can yield similar conclusions about whether or not polarization directions align.

At the other extreme, a sample's sources can converge on a hub  $H_{\min}$  that is very close to the sample. In such a case the polarization directions from different parts of the sample are different. Comparing polarization directions directly would not detect this type of alignment. The position angle histogram shows a spread out distribution of position angles, even if all the polarization directions aim toward a single point.

As an example, we consider a sample of Quasi-Stellar Objects, QSOs. The data is found in the catalog of 1450 QSOs, Pelgrims 2014 [11], which identifies QSOs in the earlier JVAS/CLASS 8.4Ghz catalog Jackson 2007 that has 12700 records. [14] These are sources of linearly polarized radio emissions.

As above, we first conduct a survey, Fig. 3, which is in the Equatorial Coordinate System. The 1450 extra-galactic radio sources populate  $5^\circ$ -radius regions each centered on a grid point of a whole-sky  $2^\circ \times 2^\circ$  grid. Compared with the alignment survey of stars, Fig. 1, one sees that the alignment of QSOs is weaker. The most significantly aligned  $5^\circ$ -radius region has significance exponent  $h = -\log_{10} S$  just over 3, while the regions in Fig. 1 for starlight have significance exponents much higher, many over 50, some as large as 250.

The sample studied here combines the QSO sources in a cluster of 14 very significantly aligned  $5^\circ$ -radius regions centered on  $(\text{RA}, \text{dec}) = (178^\circ, 10^\circ)$  near the North Galactic Pole. The most significantly aligned  $5^\circ$ -radius region is one of the 14 regions in the cluster.

The sample of partially polarized QSOs consists of 27 sources. With formulas from Sec. 3, one can

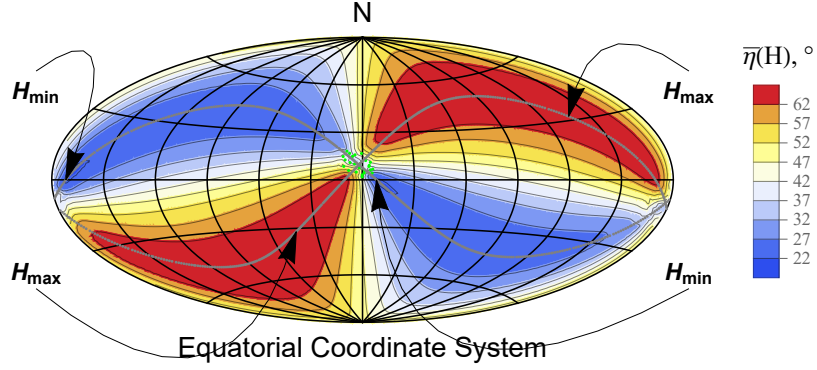


Figure 4: *The alignment function  $\bar{\eta}(H)$  for the QSO sample.* The sources are located at the green dots. As with the star sample in Fig. 2, the two Great Circles are perpendicular where they meet. Unlike Fig. 2, the QSO sample has an alignment hub  $H_{\min}$  that is so close to the sources that parallax is important. Polarization position angles  $\psi$  vary across the sample. (Equatorial coordinates, an Aitoff plot, Color online.)

calculate the alignment function  $\bar{\eta}(H)$  for this sample. The function is depicted in Fig. 4. Metrics of the alignment can be found in Tables 2 and 3. The significance of the smallest alignment angle  $\bar{\eta}_{\min}$  puts the 27-source sample better aligned than 8 random samples in a million. Hence, chance alignment is extremely unlikely.

In Fig. 4, the polarization directions determine great circles that converge at the alignment hub  $H_{\min}$  which is just  $14^\circ$  from the sample center. That means the polarization directions are not equal, but spread out in value so that they can point to  $H_{\min}$  from any location in the sample, *i.e.* they exhibit parallax. The histogram of the position angles in Fig. 5(b) shows that the PAs are evenly spread out over about  $60^\circ$ .

As noted in the literature, [7] the typical percent polarization of the QSOs is in single digits, while contamination by interstellar dust is on the order of tenths of a percent. Therefore, the physical mechanism explaining the alignment of QSO polarization directions seems to differ from the explanation of the alignment of polarized Galactic starlight.

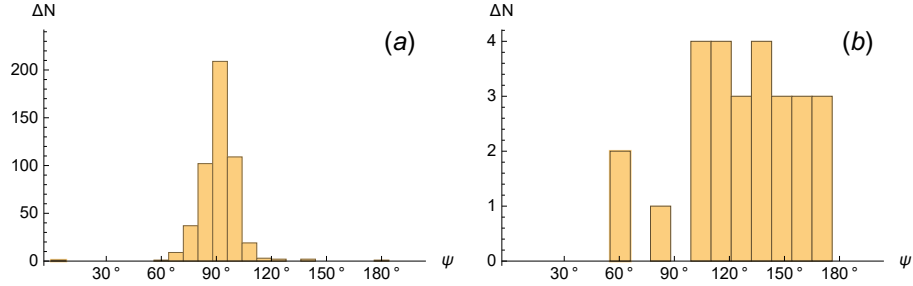


Figure 5: *Histograms of the polarization position angles  $\psi$  for (a) Stars and (b) QSOs.* (a) Stars. The position angles of the polarization directions cluster around  $\psi = 90^\circ$ , which is the position angle along the Galactic Equator to the alignment hub  $H_{\min}$  in Fig. 2. Alignment is clear from the histogram. (b) For the QSO sample, the position angle from the sample’s center toward the hub  $H_{\min}$  is  $133^\circ$  in Fig. 4. But here, parallax requires varied position angles and alignment is not clear from the  $\psi$  histogram. However, the Hub Test looks for convergence and has no trouble detecting the alignment of the polarization directions in the QSO sample, even when there is no evidence of alignment from the histogram.

### 3 The Hub Test

In general, astronomical sources are candidates for an alignment test if there is an observed asymmetry such as linear polarization or some other feature like a jet or an axis of rotation. The alignment of linear polarization directions is discussed here, but the test is easily adapted to other features. The data required to run the Hub test consists of the locations of ‘sources’  $S_i$ , each with a ‘polarization position angle’ PPA  $\psi_i$ .

The basic quantity calculated with the Hub Test is the “alignment angle”  $\eta$  of a polarization direction and the direction to a point  $H$  on the Celestial Sphere. As shown in Fig. 6, the “alignment angle”  $\eta$  separates the tangents to two Great Circles where they cross at  $S$ . One Great Circle moves away from  $S$  along the polarization direction and the other Great Circle connects  $S$  and  $H$ .

The angle  $\eta$  can be chosen to be acute because the electric field polarization direction and the tangent to the great circle from  $S$  to  $H$  are not oriented: the electric field oscillates back and forth along  $\pm\hat{\mathbf{v}}_\psi$  and both directions  $\pm\hat{\mathbf{v}}_H$  connect  $S$  to  $H$ . In (b) one sees that the alignment angle  $\eta$  can be found in the tangent plane of the source.

One should note some basic geometry. The angle  $\eta$  is the same for all points  $H'$  on the great circle connecting  $S$  and  $H$ . However, the angle  $\eta$  is undefined where either  $H$  or  $-H$  coincides with the source  $S$  or  $-S$ . There is symmetry across a diameter: Aside from the few points where it cannot be defined, the angle  $\eta$  has the same value at  $-H$  as it does at  $H$ . Also, all great circles through  $H$  contain the diametrically opposite point  $-H$ . And only  $H$  and  $-H$  are common to all the Great Circles through  $H$ . It follows that, as a function of  $H$ , the alignment angle  $\eta(H)$  is symmetric across diameters,  $\eta(H) = \eta(-H)$ .

Next, we calculate the angle  $\eta$ . All vectors in the tangent plane at  $S$ , see Fig. 6(b), are linear combinations of local North  $\hat{\mathbf{v}}_N$  and local East  $\hat{\mathbf{v}}_E$ . One can see from Fig. 6(b) that the unit vector  $\hat{\mathbf{v}}_\psi$  in the direction of  $\psi$  is the combination

$$\hat{\mathbf{v}}_\psi = \cos \psi \hat{\mathbf{v}}_N + \sin \psi \hat{\mathbf{v}}_E. \quad (2)$$

The unit vector  $\hat{\mathbf{v}}_\psi$  is on one side of  $\eta$  in Fig. 6(b).

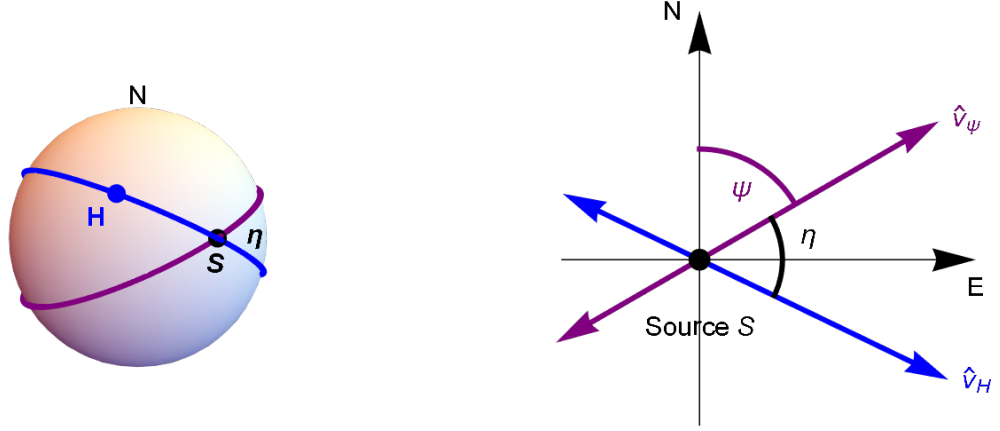


Figure 6: (Color online) A source  $S$  of polarized EM radiation and a point  $H$  are plotted on the Celestial sphere. (a) The source  $S$  and point  $H$  determine a great circle. The polarization direction is tangent to a second great circle. The angle  $\eta$  is the acute angle between the two circles at  $S$ . (b) In the plane tangent to the Celestial sphere at  $S$ , the polarization position angle PPA is an angle  $\psi$  measured clockwise from North with East to the right. The angle  $\eta$  quantifies how well the polarization direction  $\hat{v}_\psi$  aligns with the direction  $\hat{v}_H$  toward  $H$  from  $S$ .

The vector on the other side of  $\eta$  in Fig. 6(b) is the tangent to the great circle connecting  $S$  and  $H$ , the vector  $\hat{v}_H$ . Let the point  $H$  be located at  $(\text{RA}, \text{dec}) = (\alpha_H, \delta_H)$ , making sure that the point  $H$  is not  $S$  or  $-S$ . Clearly, the Great Circle containing  $H$  and  $S$  lies in the plane spanned by  $\hat{\mathbf{r}}_H$  and  $\hat{\mathbf{r}}_S$ . Since  $\hat{v}_H$  lies in the plane of the great circle, the vector must be a linear combination of  $\hat{\mathbf{r}}_H$  and  $\hat{\mathbf{r}}_S$ .

Now, since  $\hat{v}_H$  is tangent to the sphere at  $S$ , we know that  $\hat{v}_H$  is perpendicular to  $\hat{\mathbf{r}}_S$ . By applying the Gram-Schmidt process to  $\hat{\mathbf{r}}_H$  and  $\hat{\mathbf{r}}_S$ , we get  $\hat{v}_H$  from  $\hat{\mathbf{r}}_H$  by subtracting off the part of  $\hat{\mathbf{r}}_H$  that is parallel to  $\hat{\mathbf{r}}_S$ . The result is

$$\hat{v}_H = \frac{\hat{\mathbf{r}}_H - (\hat{\mathbf{r}}_S \cdot \hat{\mathbf{r}}_H)\hat{\mathbf{r}}_S}{|\hat{\mathbf{r}}_H - (\hat{\mathbf{r}}_S \cdot \hat{\mathbf{r}}_H)\hat{\mathbf{r}}_S|}, \quad (3)$$

which is a unit vector since the denominator is the length of the vector in the numerator.

With expressions for the two vectors on either side of the alignment angle  $\eta$ , one can determine  $\eta$  from the dot product of unit vectors  $\hat{v}_H$  and  $\hat{v}_\psi$ ,

$$\cos \eta = |\hat{v}_H \cdot \hat{v}_\psi|. \quad (4)$$

Since we want  $\eta$  to be the acute angle between the two directions, we employ the absolute value and require the alignment angle  $\eta$  in (4) to be restricted to the range  $0^\circ \leq \eta \leq 90^\circ$ .

Suppose we are given a sample of many sources  $S_i$ ,  $i = 1, \dots, N$ , where  $N$  is the number of sources and  $S_i$  is the location of the  $i$ th source on the sphere. The location on the Celestial Sphere is determined when we have longitude and latitude,  $(\alpha_i, \delta_i)$ . While written in conventional (RA,dec) Equatorial Coordinate System notation, the same formulas apply for the coordinates  $(l, b)$  of the Galactic Coordinate System. We used both systems, one at a time, in Sec. 2.

Each source has a polarization direction determined by a polarization position angle PPA denoted  $\psi_i$ . Then, for each point  $H$  on the sphere, there is an alignment angle  $\eta_{iH}$ , as pictured in Fig. 6 and calculated with Eq. (4), but now for each of  $N$  sources.

For almost all points  $H$  on the sphere, one can define an average alignment angle function  $\bar{\eta}(H)$  representing how well aligned with  $H$ , on average, are the polarization directions of the collection of sources  $S_i$ . Let the function  $\bar{\eta}(H)$  be defined as

$$\bar{\eta}(H) = \bar{\eta}(\alpha, \delta) = \frac{1}{N} \sum_i \eta_{iH}, \quad (5)$$

where  $(\text{RA}, \text{dec}) = (\alpha, \delta)$  is the location of  $H$ . To be more precise, this is the arithmetic mean. Plots of the function  $\bar{\eta}(\alpha, \delta)$  for the samples in Sec. 2 are displayed in Figs. 2 and 4.

Since all the alignment angles  $\eta_{iH}$  are acute angles, as noted after Eq. (4), it follows that their average, the function  $\bar{\eta}(H)$ , is also an acute angle,  $0^\circ \leq \bar{\eta}(H) \leq 90^\circ$ . Diametrical symmetry of Great Circles makes the alignment function symmetric across a diameter,  $\bar{\eta}(H) = \bar{\eta}(-H)$ .

The function  $\bar{\eta}(H)$  cannot be defined where  $H$  or  $-H$  is coincident with any of the sources,  $\pm H \neq \pm S_i$ . From Fig. 6, when  $S$  and  $H$  are the same point, infinitely many great circles ‘connect’ them, so there is no well defined angle  $\eta$ . There is a corresponding effect in the formulas;  $\hat{\mathbf{v}}_H$  in (3) is indeterminate,  $0/0$ , when  $\hat{\mathbf{r}}_H$  and  $\hat{\mathbf{r}}_S$  coincide.

The maximum and minimum values of  $\bar{\eta}(H)$  have special meanings. The Hub test provides numerical results  $\bar{\eta}_{\min}$  and  $\bar{\eta}_{\max}$  that can be used to judge how strongly the sources’ polarization directions are correlated. At points  $H$  where the function  $\bar{\eta}(H)$  is small, the great circles in the direction of the polarizations converge. Conversely, points  $H$  where  $\bar{\eta}(H)$  is high indicate divergence. The extremes are located at ‘hubs’, alignment hubs  $H_{\min}$  and  $-H_{\min}$  where the function  $\bar{\eta}(H)$  takes its minimum value and avoidance hubs  $H_{\max}$  and  $-H_{\max}$  where the alignment angle is at a maximum.

Once one has determined the smallest alignment angle  $\bar{\eta}_{\min}$  and the largest avoidance angle  $\bar{\eta}_{\max}$  for the observed data, it is important to know how likely it is that random polarization directions would have returned equivalent or better results. The intricacies of processing random polarization directions are treated in the Appendix. Similarly, basic experimental procedure produces uncertainties in every measured value. Carrying these uncertainties through the calculations produces uncertainties for the calculated results. That topic is also discussed in the Appendix.

## 4 Conclusions

Together, the examples illustrate extreme alignment. The polarized starlight converges on an alignment hub  $H_{\min}$  nearly  $90^\circ$  from the sources. As shown in Fig. 5(a), these polarized directions have position angles concentrated on a single value. The other extreme, the QSOs, has polarization directions converging close to the sources, just  $14^\circ$  way from the sample’s center. Parallax spreads out the position angles in Fig. 5(b). Both cases are very significantly aligned, but in different ways.

The star and QSO samples also differ by the significance of the alignments. The survey of QSO alignment tendencies finds correlated alignments that are much weaker than polarized Galactic starlight. The most significantly aligned  $5^\circ$ -radius QSO region is better aligned than one in 5000 randomly polarized similar samples. That level of significance makes it unlikely that alignment is due to chance. Yet, by contrast, the starlight survey has many  $5^\circ$ -radius regions in Fig. 1 that are better aligned than millions of randomly polarized samples. In Fig. 1, such regions of well-aligned polarized starlight have significance exponents  $h > 6$ , which includes most of the color dots.

Yet the degree of alignment, the percent polarization, is much stronger in the radio QSOs than in the Galactic starlight. Starlight is polarized on the order of one or two tenths of a percent, while the radio waves achieve single digits.

The unusual properties of the starlight and QSO samples that are uncovered by the Hub Test include the remarkable alignment of the polarization directions in the starlight sample; in Fig. 1 it has double the significance exponents of other similar regions. Also, for the QSOs, there is the convergence of the polarization directions so close to the sources on the sky in Fig. 4. Explaining these properties may be undertaken elsewhere.

*Acknowledgments.* My thanks to V. Pelgrims for sending me the JVAS1450 catalog that gives redshifts and identifies the QSOs among the unclassified radio sources in the JVAS/CLASS 8.4-GHz catalog. Both V. Pelgrims and N. Ridge helpfully suggested including more content than appeared in earlier versions. This research did not receive any specific grant from funding agencies in the public, commercial, or not-for-profit sectors. Conflicts of interest: none.

## References

- [1] J. L. Han, R. N. Manchester, W. van Straten, and P. Demorest. Pulsar rotation measures and large-scale magnetic field reversals in the galactic disk. *The Astrophysical Journal Supplement Series*, 234(1):11, jan 2018.
- [2] Ian W. Stephens, Leslie W. Looney, C. Darren Dowell, John E. Vaillancourt, and Konstantinos Tassis. The galactic magnetic fields effect in star-forming regions. *The Astrophysical Journal*, 728(2):99, jan 2011.
- [3] A. Lazarian and Thiem Hoang. Alignment and rotational disruption of dust. *The Astrophysical Journal*, 908(1):12, feb 2021.
- [4] Guillet, V., Fanciullo, L., Verstraete, L., Boulanger, F., Jones, A. P., Miville-Deschênes, M.-A., Ysard, N., Levrier, F., and Alves, M. Dust models compatible with planck intensity and polarization data in translucent lines of sight. *A&A*, 610:A16, 2018.
- [5] D. Hutsemekers. Evidence for very large-scale coherent orientations of quasar polarization vectors. *Astronomy and Astrophysics*, 332:410–428, April 1998.
- [6] P. Jain, G. Narain, and S. Sarala. Large-scale alignment of optical polarizations from distant QSOs using coordinate-invariant statistics. *MNRAS*, 347:394–402, January 2004.
- [7] Damien Hutsemekers, Lorraine Braibant, Vincent Pelgrims, and Dominique Sluse. Alignment of quasar polarizations with large-scale structures. *Astron. Astrophys.*, 572:A18, 2014.
- [8] Vincent Pelgrims and Damien Hutsemekers. Evidence for the alignment of quasar radio polarizations with large quasar group axes. *Astron. Astrophys.*, 590:A53, 2016.
- [9] Planck Collaboration. Planck 2018 results: XII. galactic astrophysics using polarized dust emission. *Astronomy and Astrophysics*, 641, September 2020.
- [10] Dan P. Clemens, A. F. Pinnick, M. D. Pavel, and B. W. Taylor. THE GALACTIC PLANE INFRARED POLARIZATION SURVEY (GPIPS). *The Astrophysical Journal Supplement Series*, 200(2):19, may 2012.

- [11] V. Pelgrims and J. R. Cudell. A new analysis of quasar polarization alignments. *MNRAS*, 442:1239–1248, August 2014.
- [12] Carl Heiles. 9286 Stars: An Agglomeration of Stellar Polarization Catalogs. *Astron. J.*, 119(2):923–927, February 2000.
- [13] Berdyugin, A., Piirola, V., and Teerikorpi, P. Interstellar polarization at high galactic latitudes from distant stars - viii. patterns related to the local dust and gas shells from observations of 3600 stars. *A&A*, 561:A24, 2014.
- [14] N. Jackson, R. A. Battye, I. W. A. Browne, S. Joshi, T. W. B. Muxlow, and P. N. Wilkinson. A survey of polarization in the JVAS/CLASS flat-spectrum radio source surveys - I. The data and catalogue production. *MNRAS*, 376:371–377, March 2007.
- [15] Emanuel Parzen. *Modern probability theory and its applications*. A Wiley publication in mathematical statistics. Wiley, New York, 1960.

## A Significance Level and Uncertainty

The ‘significance’ of a result means the fraction of random data sets that would give the same or a better result, *i.e.* the fraction of random runs. Hence, significance can be estimated by evaluating the results of many runs with random polarization data. Similarly, to gauge the effects of experimental uncertainty, one runs many sets of data, each set slightly off the catalog values in a way that reflects measurement uncertainties.

A random run starts by setting the number  $N$  of sources and the radius  $\rho$  of the sample region. Locate each source at a random location in the region and assign it a random PPA  $\psi$  polarization angle. Calculate the alignment angle function  $\bar{\eta}(H)$ , (5), at each grid point  $H$ . The function’s extreme values yield the alignment angle  $\bar{\eta}_{\min}$  and the alignment hub  $H_{\min}$  as well as the avoidance angle  $\bar{\eta}_{\max}$  and the avoidance hub  $H_{\max}$ .

To be able to replicate the results, we store the locations of the sources for the run, their PPA angles  $\psi$ , the location  $H_{\min}$ , the smallest average alignment angle  $\bar{\eta}_{\min}$ , the location  $H_{\max}$ , and the largest average alignment angle  $\bar{\eta}_{\max}$  are collected and stored. That completes one random run.

The sources were confined to regions of radii  $\rho = \{0^\circ, 5^\circ, 12^\circ, 24^\circ, 48^\circ, 90^\circ\}$ . By diametrical symmetry, the  $90^\circ$  region effectively covers the entire sphere. The number  $N$  of sources in each region were assigned to be  $N = \{8, 16, 32, 64, 128, 181, 256, 512\}$ . All  $6 \times 8 = 48$  cases were run  $R = 2000$  times. Table A1 has the values for the radii  $5^\circ$  and  $12^\circ$  in the text.

Thus, the probability and significance formulas are based on 48 cases of  $N, \rho$ , with each case run  $R = 2000$  times. In the text, some regions of polarized starlight are said to be better aligned than one in  $10^{150}$  or more similar regions that have randomly directed polarizations. Clearly, the assumption is made that the Gaussian tails to the fitting formulas (A-1) and (A-2) are accurate for more than  $10^{150}$  random samples. While theoretical arguments can perhaps substantiate such assumptions, no attempt is made in this article to support that assumption. Significances involving values beyond, say, one in a couple thousand should be taken as guidance.

The random runs use a  $2^\circ \times 2^\circ$  grid, or mesh. Since location is irrelevant for the random runs, the sources are confined to a single region for most of the runs, a region centered near the grid point at (RA,dec) = (71.9°, 59.4°). Sources are chosen at random from the grid points within the region and moved slightly

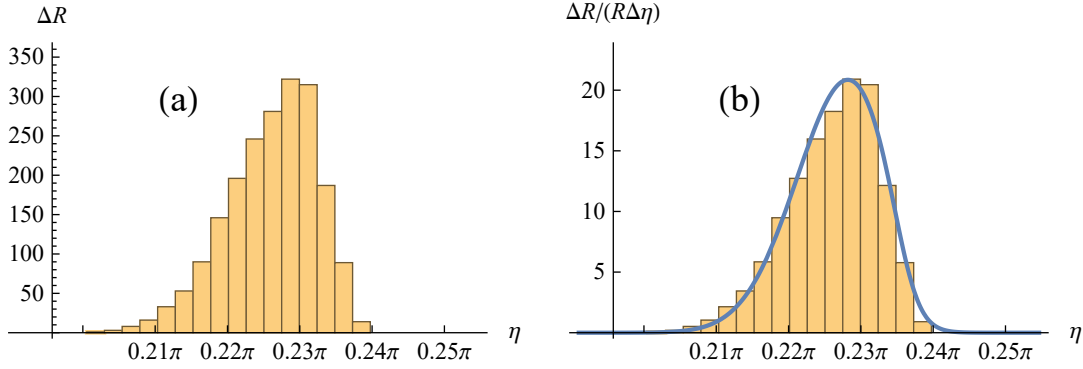


Figure A1: (Color online)  $R = 2000$  runs for  $N = 181$  sources with random polarization PPA  $\psi$ . For each run, the sources were assigned random polarization directions  $\psi$ . The best alignment angle  $\bar{\eta}_{\min}$  for each of the  $R$  runs was collected and the results analyzed. In (a), the histogram of  $\bar{\eta}_{\min}$  plots the number of runs  $\Delta R$  in each bin of width  $\Delta\bar{\eta} = 0.0025\pi$  radians. The total number of runs is the sum of the bar heights,  $R = \sum \Delta R$ . Thus, by dividing by  $R\Delta\bar{\eta}$ , the sum of the areas of the bars in (b) is unity, an approximation of the probability distribution. In the foreground is the distribution, (A-1), that fits the data, slightly steeper on the  $\eta = \pi/4 = 0.25\pi$  high side than on the low side.

off-grid to avoid resonances. However, for point-like regions with null radii,  $\rho = 0^\circ$ , the math was simpler with the sources at the North pole.

After  $R(N)$  runs with  $N$  sources, there are  $R(N)$  values of  $\bar{\eta}_{\min}$ . By counting the number  $\Delta R_i^{\min}$  of values of  $\bar{\eta}_{\min}$  that are found in an interval  $\Delta\eta$  centered on  $\eta_i$ , one obtains a histogram, the collection  $\{\eta_i, \Delta R_i^{\min}\}$ . Since the total number of runs is the sum,  $R = \sum \Delta R_i$ , the fraction of random results  $\bar{\eta}_{\min}$  that are in the  $i$ th bin is  $\Delta R_i/R$ . We have unity for the sum  $\sum_i \Delta R_i/R = 1$  and the fraction  $\Delta R_i/R$  approximates the probability of finding  $\bar{\eta}_{\min}$  with a value in the  $i^{\text{th}}$  bin.

As an example, the histogram for random runs in a region with  $N = 181$  sources is presented in Fig. A1(a). In part (b), the histogram is rescaled so that its total area is unity, just like a probability distribution.

By trying various formulas, we find one that fits the random data well. We choose

$$P^{\min}(\eta) = \frac{1.220}{\sigma\sqrt{2\pi}} \left(1 + e^{4\left(\frac{\eta-\eta_0}{\sigma}-1\right)}\right)^{-1} e^{-\frac{1}{2}\left(\frac{\eta-\eta_0}{\sigma}\right)^2}, \quad (\text{A-1})$$

where  $1.220 = \sqrt{2\pi}/\int [e^{-y^2/2}/(1+e^{4(y-1)})]dy$ . Since  $P(\eta_0 + 0.706\sigma) = P(\eta_0 - 1.018\sigma) = e^{-1/2}P(\eta_0)$ , the ‘width’ is the quantity  $0.706\sigma + 1.018\sigma = 1.72\sigma$ . The label ‘min’ in  $P^{\min}(\eta)$  indicates ‘alignment.’

The probability distribution  $P^{\min}(\eta)$  is the product of a normal distribution with a unit step, an ‘S-curve’. The S-curve is unity for small  $\eta$  and vanishes for large  $\eta$ , with a transition on the  $\pi/4$  side of the histogram. The S-curve makes the  $\eta = \pi/4$  side of the distribution steeper. See Fig. A1. Making the  $\pi/4$  side steeper pushes probability to the small  $\eta$  side. However the step function nears unity on the side of interest, the small  $\eta$  side. Since the step function is unity on the small  $\eta$  side, the side of interest behaves as a normal distribution with mean  $\eta_0$  and half-width  $\sigma$ , but with an altered normalization constant, 1.220 in place of 1.000.

To judge avoidance, the maximum angles  $\bar{\eta}_{\max}$  of the random runs were collected. All such angles exceed

$\pi/4$ . In a way that is similar to the alignment cases, one finds that the side of an avoidance histogram toward  $\eta = \pi/4$  is steeper than the far side toward  $\eta = \pi/2$ . Making the necessary adjustment to the formula, two sign changes compared with (A-1), the random results can be fit with an avoidance probability distribution  $P^{\max}(\eta)$  given by

$$P^{\max}(\eta) = \frac{1.220}{\sigma\sqrt{2\pi}} \left(1 + e^{-4\left(\frac{\eta-\eta_0}{\sigma}+1\right)}\right)^{-1} e^{-\frac{1}{2}\left(\frac{\eta-\eta_0}{\sigma}\right)^2} . \quad (\text{A-2})$$

As with alignment, the side of interest, the side toward  $\eta = \pi/2$ , is where the step function becomes unity and the function is a normal distribution but with a scaling factor of 1.220 in place of 1.000 .

By fitting probability distributions (A-1) and (A-2) to histograms for  $R(N)$  random runs in a region of radius  $\rho$ , one finds a mean value  $\eta_0(N)$  and a half-width  $\sigma(N)$  for each  $N$  and  $\rho$ . It turns out that the various  $\eta_0(N)$  and  $\sigma(N)$  are well described by simple functions of  $\sqrt{N}$ ,

$$\begin{aligned} \eta_0^{\min}(N) &= \frac{\pi}{4} - \frac{c_1}{(\sqrt{N})^{a_1}} \approx \frac{\pi}{4} - \frac{1}{\sqrt{N}} \quad ; \quad \sigma^{\min}(N) = \frac{c_2}{4(\sqrt{N})^{a_2}} \approx \frac{1}{4\sqrt{N}} \\ \eta_0^{\max}(N) &= \frac{\pi}{4} + \frac{c_1}{(\sqrt{N})^{a_1}} \approx \frac{\pi}{4} + \frac{1}{\sqrt{N}} \quad ; \quad \sigma^{\max}(N) = \frac{c_2}{4(\sqrt{N})^{a_2}} \approx \frac{1}{4\sqrt{N}} \end{aligned} \quad (\text{A-3})$$

where the parameters  $c_i$  and  $a_i$ , for  $i = \{1, 2\}$  and  $\eta_0^{\min}$  and  $\eta_0^{\max}$ , depend  $\rho$ . See Table 1. Many values are near unity and the simpler expressions in (A-3) apply when the parameters  $a_i$  and  $c_i$  are equal to one.

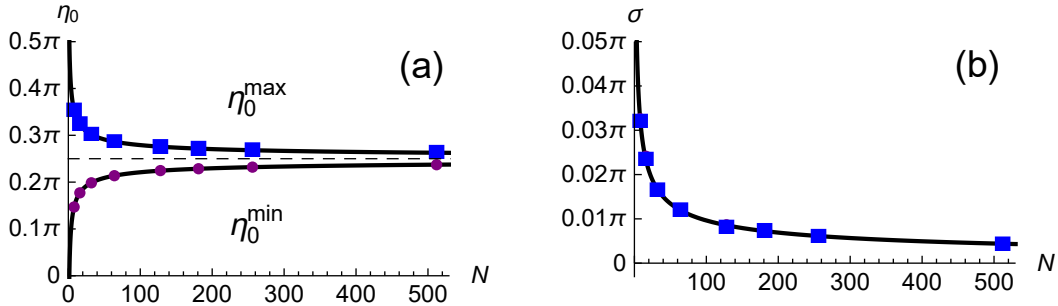


Figure A2: (Color online) *The mean  $\eta_0$  and half-width  $\sigma$  parameters for random runs as functions of the number of sources  $N$  in (A-3) and Table 1. (a) Note that avoidance (max) and alignment (min) are symmetric about the dashed line where the angle is  $0.25\pi = 45^\circ$ . (b) Since, for  $\rho > 5^\circ$ , the parameters  $c_i, a_i$  are roughly unity,  $c_i, a_i \approx 1$ , the half-widths  $\sigma$  are about  $1/(4\sqrt{N})$ , which, by (A-3), is a quarter of the separation of the  $\eta_0$  curves in (a) from the dashed center line  $\eta_0 = \pi/4$ .*

With random data, the sum on the right in (5) is a sum of random numbers constrained to the interval  $[0, \pi/2]$  with a mean value of  $\pi/4$ . One can show that the dependence on  $\sqrt{N}$  of  $\eta_0^{\min}(N)$  and  $\eta_0^{\max}(N)$  in (A-3) can be made plausible by adapting random walk ideas. [15]

Region Radius $\rho$	$c_1^{\min}$	$a_1^{\min}$	$c_2^{\min}$	$a_2^{\min}$
12°	$0.8912 \pm 0.0034$	$1.0054 \pm 0.0026$	$1.238 \pm 0.039$	$1.021 \pm 0.021$
5°	$0.8363 \pm 0.0035$	$1.0088 \pm 0.0028$	$1.076 \pm 0.030$	$0.940 \pm 0.019$
Region Radius	$c_1^{\max}$	$a_1^{\max}$	$c_2^{\max}$	$a_2^{\max}$
12°	$0.9049 \pm 0.0069$	$1.0090 \pm 0.0052$	$1.228 \pm 0.039$	$1.018 \pm 0.022$
5°	$0.8424 \pm 0.0038$	$1.0062 \pm 0.0031$	$1.168 \pm 0.022$	$0.992 \pm 0.013$

Table A1: Parameters  $c_i$  and  $a_i$ ,  $i = 1, 2$  in (A-3) for regions with radii  $\rho = 5^\circ, 12^\circ$ .

Given an ‘observed’ alignment angle  $\bar{\eta}_{\min}^{\text{obs}}$ , *i.e.* one that is calculated from observed polarizations, there is a chance that randomly directed polarizations can produce an equal or smaller alignment angle. The “significance”  $S$  of a particular  $\bar{\eta}_{\min}^{\text{obs}}$  is defined to be the likelihood that random runs will show better alignment than indicated by the observed angle.

Similarly, there is a likelihood that the avoidance angle  $\bar{\eta}_{\max}^{\text{obs}}$  could be less than the result with some randomly aligned sample. We therefore define two significances  $S^{\min}(\bar{\eta}_{\min}^{\text{obs}})$  and  $S^{\max}(\bar{\eta}_{\max}^{\text{obs}})$ , one for alignment and one for avoidance.

Given the approximations  $P(\eta)$  in (A-1) and (A-2) to the probability distributions, the significance of an alignment or avoidance angle  $\bar{\eta}^{\text{obs}}$  is approximated by the integral from/to infinity,

$$S^{\min}(\bar{\eta}_{\min}^{\text{obs}}) = \int_{-\infty}^{\bar{\eta}_{\min}^{\text{obs}}} P^{\min}(\eta) d\eta \quad ; \quad S^{\max}(\bar{\eta}_{\max}^{\text{obs}}) = \int_{\bar{\eta}_{\max}^{\text{obs}}}^{\infty} P^{\max}(\eta) d\eta \quad . \quad (\text{A-4})$$

The significance formula for an observed min alignment angle  $\bar{\eta}_{\min}^{\text{obs}}$  is the fraction of random runs that would yield better alignment, *i.e.* a smaller alignment angle  $\bar{\eta}_{\min}$ . Similarly, the significance formula for an observed max avoidance angle  $\bar{\eta}_{\max}^{\text{obs}}$  in (A-4) indicates the likelihood that random runs would produce larger avoidance angles than the angle  $\bar{\eta}_{\max}^{\text{obs}}$  that is calculated from observed data.

Note that the distributions in (A-1) and (A-2) have nonzero values for any real  $\eta$ , positive or negative. But the scaled histograms that the distributions fit are confined to the finite interval  $0^\circ \leq \eta \leq 90^\circ$ , since the alignment and avoidance angles  $\bar{\eta}_{\min}$  and  $\bar{\eta}_{\max}$  are nonnegative acute angles. So, there might be a problem.

Probabilities and significances are meaningless for alignment angles that are negative,  $\bar{\eta} < 0^\circ$ , or larger than a right angle,  $\bar{\eta} > 90^\circ = \pi/2$  radians. Ignoring the small differences due to the parameters  $c_i$  and  $a_i$ , by (A-4), we have  $S_N^{\min}(0) \approx S_N^{\max}(\pi/2)$ , which means that the significances of the disallowed angles smaller than 0 and larger than  $90^\circ = \pi/2$  are about the same. For  $N = 4$  sources in  $24^\circ$  radius regions, one calculates  $S_{N=4}^{\min}(0) \approx S_{N=4}^{\max}(\pi/2) = 0.014$ , which is more than 1% and is not negligible when determining significance. Upon increasing number of sources to  $N = 7$ , one finds that  $S_{N=7}^{\min}(0) \approx S_{N=7}^{\max}(\pi/2) = 4 \times 10^{-5}$  or 0.004%. That may be considered negligible. Thus, to avoid inaccurate significance values with small numbers of sources, only regions with seven or more sources are considered.